Available online at www.sciencedirect.com
SCIENCE DIRECT
Thermochimica Acta 439 (2005) 80–85
thermochimica acta
www.elsevier.com/locate/tca

Thermal behaviour of polyoxocarbosilane shells in Fe-based (core)–polyoxocarbosilane (shell) nanocomposites

A. Galíková [a], Z. Bastl [b], R. Alexandrescu [c], I. Morjan [c], J. Pola [a,*]

[a] *Laboratory of Laser Chemistry, Institute of Chemical Process Fundamentals, Academy of Sciences of the Czech Republic, 6-Suchdol, 16502 Prague, Czech Republic*
[b] *J. Heyrovský Institute of Physical Chemistry, Academy of Sciences of the Czech Republic, 18223 Prague, Czech Republic*
[c] *National Institute for Lasers, Plasma and Radiation Physics, R-76900 Bucharest, Romania*

Received 16 May 2005; received in revised form 9 August 2005; accepted 5 September 2005
Available online 13 October 2005

Abstract

Thermal behaviour of Fe-based (Fe/Fe_2O_3 core)–polyoxocarbosilane (shell) nanocomposites, prepared by laser-induced co-decomposition of iron pentacarbonyl and hexamethyldisiloxane in the gas phase, was examined by using TGA technique. The thermal decomposition of the polymer shell of the nanocomposite is revealed as a two-stage (low- and high-temperature) evolution of methane. The importance of the low-temperature stage increases and that of the high-temperature stage decreases with increasing amount of the Fe/Fe_2O_3 cores. The results represent the first thermal data related to nanocomposite metal/polymer system and are explained in terms of heterogeneous catalysis of the polyoxocarbosilane decomposition by the Fe/Fe_2O_3 core.

Keywords: Thermal decomposition; Iron/polyoxocarbosilane nanocomposite; TGA; Heterogeneous effect

1. Introduction

Iron- and iron oxide-based nanocomposite materials with iron or iron oxide nanoparticles separated by different insulating media as porous glass [1], mesoporous silica [2], silicon oxide [3] and various polymers [4–7] have been of great interest due to their superparamagnetic properties [8] and potential applications in medical diagnostic technologies [9,10] and sensors and actuators systems [11–14].

The nanosized particles of iron stabilized by polymers were prepared by sonolysis of iron pentacarbonyl in the presence of poly(dimethylphenyleneoxide) [15] and those of iron oxide embedded in organic polymers were prepared by static casting [16], ultrasound radiation [17], wet chemical approach [18], seed precipitation–polymerization in the presence of iron oxide nanoparticles [19], in situ oxidation of iron salts within polymer latex [20], and laser-induced formation of cationic particles acting as polymerization catalysts [21].

We have recently reported that IR laser ethylene-sensitized heating of gaseous iron pentacarbonyl-hexamethyldisiloxane [22,23] (or methoxytrimethylsilane, [24]) results in the formation of nanosized iron-based particles that are covered with organosilicon polymer and which become superficially oxidized to Fe_2O_3 through incomplete protection by or porous structure of the surrounding polymer. Having been produced at high-temperatures and incorporating γ-Fe_2O_3 (and α-Fe_2O_3) in the outer core phase, these nanocomposites show ferromagnetic and superparamagnetic properties and high specific surface area and can be therefore promising as nanostructured magnetic ceramics [25] and high-temperature gas sensors [13].

These materials can also serve as an interesting model for examination of the effect of the Fe/Fe_2O_3 core on the decomposition of the polymeric shell. Conventional thermal degradation of polymers is, in principle, affected (e.g. [26]) by ubiquitous heterogeneous, surface-catalyzed steps, whose real importance was recently manifested through achieving decomposition of several polymers upon irradiating them by using IR lasers (e.g. [27–29]). The examination of the organosilicon polymer degradation in the Fe/Fe_2O_3 (core)/polyoxocarbosilane (shell) system can not only reveal the effect of the Fe/Fe_2O_3 core on the mode

* Corresponding author. Tel.: +420 2 20390308; fax: +420 2 20920661.
E-mail address: pola@icpf.cas.cz (J. Pola).

0040-6031/$ – see front matter © 2005 Elsevier B.V. All rights reserved.
doi:10.1016/j.tca.2005.09.002

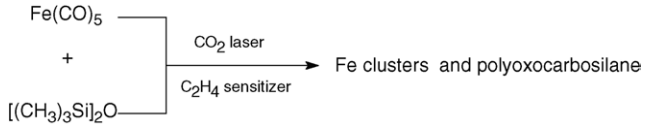

Scheme 1.

and feasibility of the decomposition of the polymer shell, but also verify the presumed thermal stability and hence potential of these nanocomposites for their use as high-temperature sensors.

In this work we extend our previous results on laser-synthesis of Fe/Fe_2O_3 (core)–polymer (shell) nanocomposites [22–24] and report on thermal behaviour of these materials.

2. Experimental

2.1. Materials

The black nanosized composites possessing Fe core (having Fe_2O_3 in outer layers) embedded in polyoxocarbosilane were produced by IR laser irradiation of gaseous iron pentacarbonyl and hexamethyldisiloxane (Scheme 1) as described elsewhere [22].

Briefly, the vapors of iron pentacarbonyl and hexamethyldisiloxane (each diluted with ethene) together with argon (needed for gas and particle confinement) were separately introduced into the reaction chamber through three concentric nozzles at different flow rates of $Fe(CO)_5/C_2H_4$ and $[(CH_3)_3Si]_2O/C_2H_4$ and different total pressures (Table 1). The flow rates of $Fe(CO)_5/C_2H_4$, $[(CH_3)_3Si]_2O/C_2H_4$ and Ar were controlled by PTFE valves and mass flow controllers.

The laser beam (output power 80 W, $\lambda = 10.6\,\mu m$) mildly focused to achieve an energy density of 2 kW/cm^2 when crossed with the reactant flow enabled to yield ca. 1 g of an ultrafine black powder after 1 h irradiation. The experimental conditions of the nanocomposites synthesis are given in Table 1.

The black fine powders are easily handled except for that obtained in Run 1, whose manipulation is, similarly to ultrafine polyoxocarbosilane powders produced by IR laser-induced decomposition of disiloxanes [30], difficult because of its electrostatic charge.

2.2. Thermal analysis

Thermal analysis of the Fe/polyoxocarbosilane nanocomposites (sample weight (12–20 mg) was carried out by heating the samples up to 750 °C at the rate of 4 °C/min using Cahn D-200 recording microbalances in a stream of argon (flow rate 100 ml/min). The composition of the outgoing gas was analyzed by an automatic sampling gas chromatograph Hewlett-Packard GC5890 equipped with FID and TCD detectors and Porapak P packed column (i.d. 2 mm, length 2 m) and by mass spectrometer (a VG GAS Analysis Ltd., spectrometer) running in multiple ion monitoring mode (selection of 16 specific ions displayed as a time-dependent plot). The quantification of the chromatographic data was made using streams of argon mixed with amounts of authentic samples as controlled by mass flow AFC 2600 controllers (Aalborg instruments Inc.).

2.3. Physical methods used for characterization of materials

The laser-produced nanocomposites and the materials obtained from them after heating to 750 °C were characterized by X-ray photoelectron (XPS) and FT-IR spectroscopy and transmission electron microscopy.

X-ray photoelectron spectra (XPS) were measured with a Gammadata Scienta ESCA 310 electron spectrometer using monochromatized Al Kα ($h\nu = 1486.6$ eV) radiation for electron excitation. The energy scale of the spectrometer was calibrated with Au $4f_{7/2}$ binding energy fixed at 84.0 eV. The high resolution spectra of Fe 2p, Si 2p, Si 2s, C 1s and O 1s photoelectrons were measured for a sample as received. The ratios of atomic elemental concentrations were calculated assuming homogeneous sample.

The FT-IR spectra (a Nicolet Impact spectrometer) were taken for materials in a KBr pellet.

TEM photomicrographs on samples scrubbed from the reactor surface and held with a copper grid were obtained using a Philips 201 transmission electron microscope.

Table 1
Experimental conditions for synthesis of and Fe content in the nanocomposites

Run	Flow rate (sccm)				P_{total}[a] (mbar)	Wt.% of Fe in nanocomposite[b]
	C_2H_4[c]	$Fe(CO)_5$	C_2H_4[d]	$[(CH_3)_3Si]_2O$		
1	60	4.67	30	0.95	650	32
2	60	5.60	30	1.13	550	45
3	60	7.00	40	1.39	450	63
4	60	7.00	50	1.39	450	65
5	60	7.00	30	1.39	450	73
6	60	7.00	30	1.39	450	76

[a] $Fe(CO)_5 + [(CH_3)_3Si]_2O$ + ethene + Ar.
[b] Elemental analysis.
[c] Used for dilution of $Fe(CO)_5$.
[d] Used for dilution of $[(CH_3)_3Si]_2O$.

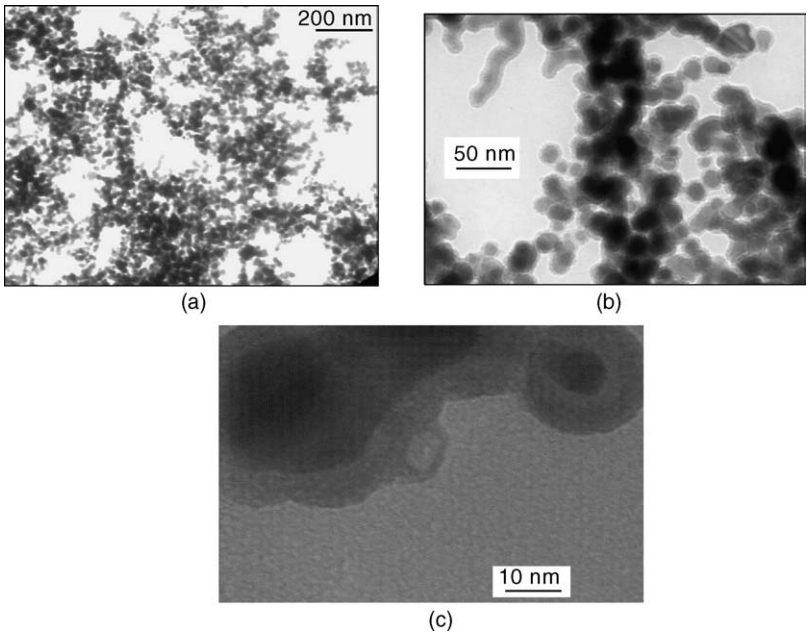

Fig. 1. Typical TEM images of Fe/Fe_2O_3/polyoxocarbosilane nanocomposite (the examples given relate to Run 4).

3. Results and discussion

3.1. Structure of initial nanocomposites

The structure of the nanocomposites differring by the content of Fe in them (Table 1) corresponds to agglomerated chains of ca. 20–100 nm in diameter (Fig. 1), which consist of dark cores and a lighter shell phase, respectively, attributed [23] to the elemental iron/iron oxide and polyoxocarbosilane.

Although their X-ray photoelectron spectra reveal small differences in the abundance of O and C in their superficial layers, the bulk composition indicated by the FT-IR spectra is rather similar. The FT-IR spectra of all samples show typical pattern [30,31] of polyoxocarbosilanes containing contributions of ν(Si–O–X, X = Si, C) at 980–1180 cm^{-1}, ν(C–H) at 2850–2960 cm^{-1}, and ν(C=C) at ~1630 cm^{-1}. The relative absorbance of the ν(C–H) and ν(Si–O–X) band, the $A_{(C–H)}/A_{(Si–O–X)}$ ratio decreases going from Run 1 to Run 6 (0.32 (Run 1) 0.11 (Run 2), 0.08 (runs 3 and 4) and 0.05 (runs 5 and 6)), which indicates that the lower Fe content corresponds to more abundant C–H bonds.

3.2. Thermal decomposition of nanocomposites

The heating of the Fe-based (core)–polyoxocarbosilane (shell) nanocomposites (Table 1) to 750 °C does not lead to any change of their appearance — the powders remain easily handled and retain their black color and TEM images (Fig. 2).

Thermograms of the samples reveal that the powders stability remarkably depends on the Fe/Fe_2O_3 content in them (Fig. 3). The polymer shells in the powders with Fe content 32 and 45 wt.% decrease their weight by ca. 15 wt.% only, whereas those in the powders with Fe content 63 and 65 wt.%, respectively, deplete by ca. 35 and 45 wt.%, and those in the powders possessing 73 and 75 wt.% Fe decrease their weight by almost 60 and 65%. Although these differences can be to some extent related to slight differences in structure and H content of the polymer shell, they clearly manifest that the polymer shell degradation is enhanced with higher content of the Fe/Fe_2O_3 component (Fig. 4).

We assume that the weight decrease at around 100 °C is likely due to desorption of traces of omnipresent water. That at higher temperatures is very mostly due to evolution of methane.

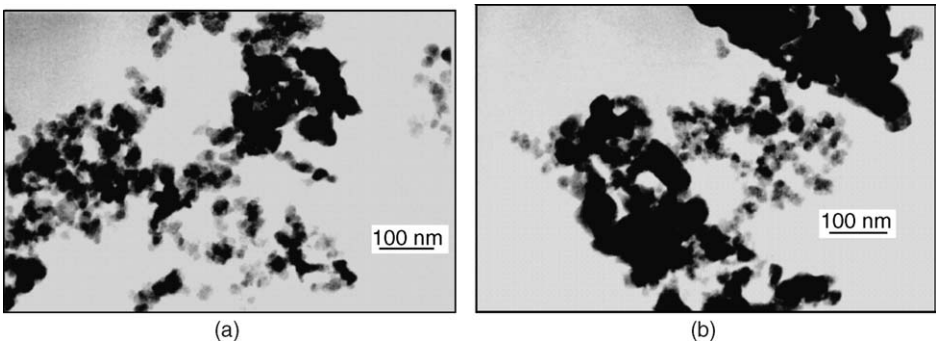

Fig. 2. TEM images of TGA-treated Fe/Fe_2O_3/polyoxocarbosilane nanocomposite from runs 4 (a) and 6 (b).

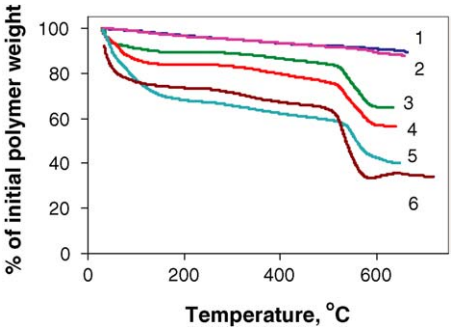

Fig. 3. Thermograms of the Fe/Fe_2O_3/polyoxocarbosilane nanocomposite powders obtained from runs 1–6. (The numbers correspond to run designation in Table 1.)

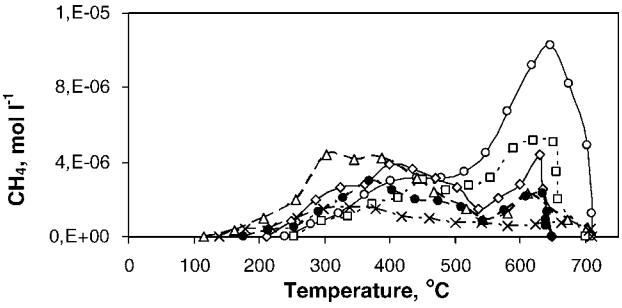

Fig. 5. Evolution of methane in thermal decomposition of Fe/polyoxocarbosilane nanocomposites produced from Run 1 (◯), 2 (□), 3 (◊), 4 (♦), 5 (×) and 6 (△).

The other observed products are ethane, hydrogen, methylsilane and carbon oxides. Except for ethane (ca. 8 mol% of methane) evolved in the thermal degradation of the nanocomposite from Run 1, all these compounds are produced in amounts by at least of two orders of magnitude lower. The observed preponderance of methane is in line with cleavage of $Si–CH_3$ bonds giving rise to $CH_3^{\cdot}$ radicals and with abstraction of H by this radical from the polymer. These steps generate unsaturated Si centers that are capable of inducing rearrangements and cleavages in polymer skeleton. The plausible reactions are [32] cleavage to silanone and small Si-centered radicals, the disproportionation of the latter to silene and methylsilanes, silylene formation and scrambling of Si–C and Si–O bonds. Other likely reactions are formation of relatively stable C=C and very unstable Si=C bonds that are reactive [33] towards oxygen and air moisture. The latter induces changes in polymer structure on air due to formation of Si–O and C=O bonds [33] as observed by IR and XP spectra.

The evolution of methane is a two-stage process characterized with the evolution maxima at ca. 350 and 650 °C (Fig. 5). Very interestingly, the relative importance of these stages (ratio of areas under the appropriate parts of curve) is affected by the Fe/Fe_2O_3 content in the nanocomposite, the second stage growing in importance with decreasing Fe/Fe_2O_3 content (Fig. 6).

3.3. Changes in nanocomposites structure

The FT-IR spectra of the heated samples resemble those of the initial ones, the only noticeable difference being a small ($\sim$10–20 cm^{-1}) shift of the intense ν(Si–O–X, X = Si, C) band to higher wave numbers. Such changes in linear siloxanes relate [34] to decreasing size, branching or increasing number of O atoms bonded to silicon.

The interpretation of the above dependences is, however, helped by the comparison of the X-ray photoelectron spectra taken before and after TGA of the superficial layers of those nanocomposites (Table 2), which differ most in the Fe content (runs 1 and 6). The Fe (2p) spectra reveal [35,36] the presence of two chemical states of iron i.e. that of Fe^0 (707.5 eV) and Fe^{3+} (Fe_2O_3, 711.5 eV). They also show that the outer layers of the Fe-richer sample contain both contributions, but those of the Fe-poor sample contain only the oxidized form. (The presence of both states in the deeper layers of the samples was, however, confirmed by Ar ion sputtering [22,23]). The spectra of the Si (2p) electrons resemble those of ultrafine polyoxocarbosilane powders obtained by laser-induced gas phase decomposition of hexamethyldisiloxane [35,37] and can be decomposed into two components at 102.2 and 103.4 eV, which respectively correspond [38,39] to $CSiO_x$ ($x = 2, 3$) and SiO_4 structural units. The C (1s) spectra can be decomposed into components at 284.8, 286.7 and 289.2 eV which are assignable [40] to CH_x, C–O and O=C–O (resp. C–O–C) moieties. The O (1s) spectra are represented [40] by O^{2-}, O(=C–O), OH, O–SiC and C–O–X (X=C, H) and SiO_4 components.

The relative abundances of these components calculated from intensities of Si (2s), Fe (2p), C (1s) and O (1s) photoemission

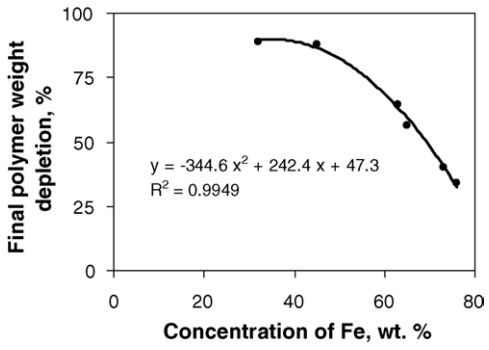

Fig. 4. Dependence of the polymer weight depletion on the Fe/Fe_2O_3 content in the Fe/Fe_2O_3/polyoxocarbosilane nanocomposite.

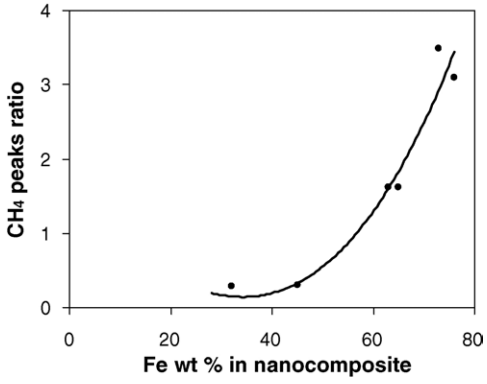

Fig. 6. Dependence of the first to second stage of methane evolution on the Fe/Fe_2O_3 content in the Fe/Fe_2O_3/polyoxocarbosilane nanocomposite.

Table 2
Chemical composition (normalized to atomic concentration of Si; the Si, Fe, C and O spectra were assigned after [35–40]) of the nanocomposites before (B) and after (A) TGA as calculated from integral intensities of Si (2s), Fe (2p), C (1s) and O (1s) lines

Sample from run	Stoichiometry	Si		Fe		C			O		
		R–Si–O	SiO_4	Fe^0	Fe^{3+}	CH_x	C–OH C–O	O=C–O C–O–C	O^{2-}	O^*=C–O R–Si–O	OH^- O=C–O^* C–O–C C–OH SiO_4
1 B	$Si_{1.00}Fe_{0.16}O_{1.62}C_{1.38}$	0.49	0.51	0.16		1.26	0.09	0.03	0.20	0.52	0.90
1 A	$Si_{1.00}Fe_{0.18}O_{2.22}C_{0.85}$	0.35	0.65	0.18		0.79	0.02	0.04	0.32	0.80	1.10
6 B	$Si_{1.00}Fe_{0.83}O_{3.26}C_{2.54}$	0.68	0.32	0.38	0.45	2.09	0.21	0.24	1.44	1.00	0.83
6 A	$Si_{1.00}Fe_{0.69}O_{3.62}C_{0.77}$	0.61	0.40	0.01	0.68	0.61	0.08	0.08	1.69	0.97	0.94

lines show that both *laser-produced samples* have more CH_x moieties than CH structures bonded to O. Additionally, the Fe-rich sample has more C, O and $CSiO_x$ units (compared to SiO_4 units). It also appears that the *TGA-derived samples* (samples heated to 750 °C) decrease their C content and increase their O content and that the heating of the Fe-rich sample leads to more C depletion but lower O uptake.

These spectral changes confirm that the TGA of the nanocomposites can be accounted for by depletion of carbon, which is in line with the observed evolution of methane and which leads to the formation of the SiO_x structures with $n > 2$ together with O-containing carbonaceous units.

The two-stage of the thermal decomposition of the polyoxocarbosilane shell in the Fe/Fe_2O_3/polyoxocarbosilane nanocomposite are in keeping with the occurrence of two different mechanisms. More feasible low-temperature decomposition facilitated at higher Fe/Fe_2O_3 content strongly suggests the presence of heterogeneous effects, i.e. a Fe and/or Fe_2O_3 catalysis of the Si–C bond cleavage taking place in polymer layers that are in direct contact to the core. Iron and iron oxides are considered as low-efficient catalysts [41] and it is possible that the catalysis involves nanosized features and/or surface defects. The high-temperature decomposition presumably occurs with polymer not being in a direct contact with the core. This view is supported by the fact that this stage becomes more pronounced with decreasing Fe/Fe_2O_3 content. The two different degradation stages are illustrated in Scheme 2. The scheme is supported by the previously observed methane evolution at ∼650 °C from nanosized polyoxocarbosilane powders not containing Fe/Fe_2O_3, [30,32].

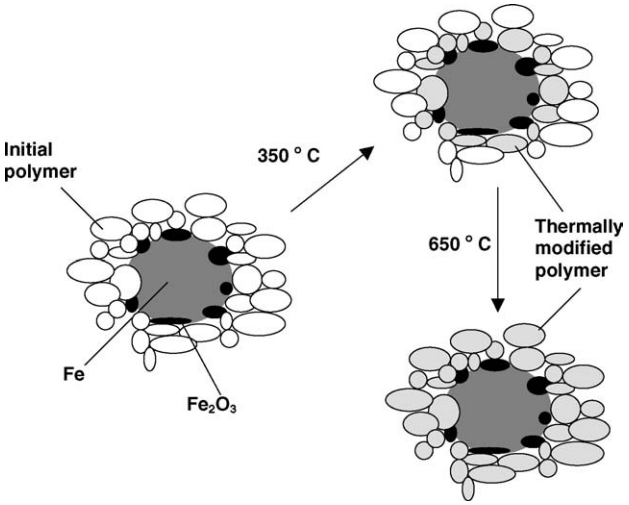

Scheme 2. Two state decomposition of the polyoxocarbosilane shell in the Fe/Fe_2O_3 (core)/polyoxocarbosilane (shell) nanocomposite.

4. Conclusion

Thermal decomposition of the polyoxocarbosilane shell in the Fe/Fe_2O_3/polyoxocarbosilane nanocomposite, produced by laser-induced co-decomposition of iron pentacarbonyl and hexamethyldisiloxane in the gas phase, revealed that the polymer evolves methane as a dominant product and that it degrades via two different stages peaking at 350 and 650 °C.

The observed dependence of the methane evolution in the low- and high-temperature stages on the Fe/Fe_2O_3 content and the assigned structural changes in the heated polymer are consistent with each stage occurring through different mechanism.

The low-temperature stage occurring at 350 °C involves heterogeneous catalysis by the Fe/Fe_2O_3 core and the high-temperature stage taking place at 650 °C resembles the previously reported thermal degradation of polyoxocarbosilanes and can be considered as homogeneous process.

These results represent the first thermal degradation data related to nanocomposite metal/polymer system and indicate specific features of thermal degradation of these materials which presently attract so much interest [42–45].

Acknowledgements

Research was supported by NATO Collaborative Research Grant CLG 98058 and by GACR (grant no. 104/04/2028). We thank Mr. E. Macháčková for the Fe analysis and Dr. G. Prodan and Dr. J. Boháček for the TEM analysis.

References

[1] N.F. Borelli, D.L. Morse, J.W.H. Schreurs, J. Appl. Phys. 54 (1983) 3344.
[2] M. Fröba, R. Köhn, G. Bouffaud, O. Richard, G. van Tendeloo, Chem. Mater. 11 (1999) 2858.
[3] R.D. Shull, J.J. Ritter, L.J. Swartzendruder, J. Appl. Phys. 69 (1991) 5144.
[4] L. Chen, W.J. Yang, C.Z. Yang, J. Mater. Sci. 32 (1997) 3571.
[5] M. Kryszewski, J.K. Jeszka, Synthetic Met. 94 (1998) 99.
[6] R.F. Ziolo, E.P. Giannelis, B.A. Weinstein, M.P. O'Horo, B.N. Ganguly, V. Mehrotra, M.W. Russell, D.R. Huffman, Science 257 (1992) 219.
[7] H. Okada, K. Sakata, T. Kunitake, Chem. Mater. 2 (1990) 89.
[8] R.D. Shull, L.H. Bennett, Nanostruct. Mater. 1 (1992) 83.

[9] N.M. Pope, R.C. Alsop, Y.-A. Chang, A.K. Smith, J. Biomed. Mater. Res. 29 (1994) 449.
[10] A. Petri-Fink, M. Chastellain, L. Juillerat-Jeanneret, A. Ferrari, H. Hofmann, Biomaterials 26 (2005) 2685.
[11] D.-D. Lee, D.-H. Choi, Sens. Actuators B 1 (1990) 231.
[12] V.V. Malyshev, A.V. Eryshkin, E.A. Koltypin, A.E. Varfolomeev, A.A. Vasiliev, Sens. Actuators B 18 (1994) 434.
[13] J.S. Han, T. Bredow, D.E. Davey, A.B. Yu, D.E. Mulcahy, Sens. Actuators B 75 (2001) 18.
[14] Z. Tianshu, L. Hongmei, Z. Huanxing, Z. Ruifang, S. Yusheng, Sens. Actuators B 32 (1996) 181.
[15] D. de Caro, T.O. Ely, A. Mari, B. Chaudret, Chem. Mater. 8 (1996) 1987.
[16] B.H. Sohn, R.E. Cohen, Chem. Mater. 9 (1997) 264.
[17] R.V. Kumar, Yu. Koltypin, Y.S. Cohen, Y. Cohen, D. Aurbach, O. Palchik, I. Felner, A. Gedanken, J. Mater. Chem. 10 (2000) 1125.
[18] C.R. Mayer, V. Cabuil, T. Lalot, R. Thouvenot, Angew. Chem. Int. Ed. Engl. 38 (1999) 3672.
[19] P.A. Dresco, V.S. Zaitsev, R.J. Gambino, B. Chu, Langmuir 15 (1999) 1945.
[20] K.S. Nustad, T.E. Funderud, A. Berge, J. Ugelstad, in: F. Candau, R.H. Ottewill (Eds.), Scientific Methods for the Study of Polymer Colloids and their Applications, Kluwer Academic, Dordrecht, 1990, p. 517.
[21] M.S. El-Shall, Appl. Surf. Sci. 106 (1996) 347 (and refs. therein).
[22] J. Pola, M. Maryško, V. Vorlíček, Z. Bastl, A. Galíková, K. Vacek, R. Alexandrescu, F. Dumitrache, I. Morjan, L. Albu, G. Prodan, Appl. Organometal. Chem. 19 (2005) 1015.
[23] R. Alexandrescu, F. Dumitrache, I. Morjan, M. Maryško, K. Vacek, Z. Bastl, J. Pola, in preparation.
[24] J. Pola, Z. Bastl, V. Vorlíček, F. Dumitrache, R. Alexandrescu, I. Morjan, I. Sandu, V. Ciupina, Appl. Organometal. Chem. 18 (2004) 337.
[25] A. Dumitru, A. Morozan, C. Mirea, D. Mihaiescu, C. Panaiotu, V. Ciupina, I. Stamatin, Compos. Sci. Technol. 65 (2005) 713 (and refs. therein).
[26] D.L. Chinaglia, R. Hessel, O.N. Oliviera, Polym. Degrad. Stabil. 74 (2001) 97.
[27] J. Pola, J. Kupčík, S.M.A. Durani, E.E. Khawaja, H.M. Masoudi, Z. Bastl, J. Šubrt, Chem. Mater. 15 (2003) 3887.
[28] J. Kupčík, J. Blazevska-Gilev, J. Pola, Macromol. Rapid Commun. 26 (2005) 386.
[29] S.M.A. Durani, E.E. Khawaja, H.M. Masoudi, Z. Bastl, J. Šubrt, A. Galíková, J. Pola, J. Anal. Appl. Pyrol. 73 (2005) 145.
[30] J. Pola, A. Ouchi, K. Vacek, A. Galíková, V. Blechta, J. Boháček, Solid State Sci. 5 (2003) 1079.
[31] J. Pola, R. Tomovska, S. Bakardjieva, A. Galíková, K. Vacek, A. Galík, J. Non-Crystal. Solids 328 (2003) 227.
[32] J. Pola, A. Galíková, A. Galík, V. Blechta, Z. Bastl, J. Šubrt, A. Ouchi, Chem. Mater. 14 (2002) 144 (and refs. therein).
[33] J. Pola, J. Vítek, Z. Bastl, J. Šubrt, J. Organometal. Chem. 640 (2001) 170.
[34] Infrared Structural Correlation Tables and Data Cards, Heyden and Son Ltd., Spectrum House, London, 1969.
[35] NIST. X-ray Photoelectron Spectroscopy Database, ver. 2.0, US Department of Commerce, NIST, Gaithersburg, MD 20899, USA, 1997.
[36] B.J. Tan, K.J. Klabunde, P.M. Sherwood, Chem. Mater. 2 (1990) 186.
[37] J. Kupčík, Z. Bastl, J. Šubrt, J. Pola, V.C. Papadimitriou, A.V. Prosmitis, P. Papagiannakopoulos, J. Anal. Appl. Pyrol. 57 (2001) 109.
[38] M.R. Alexander, R.D. Short, F.R. Jones, M. Stollenwerk, J. Zabold, W. Michaeli, J. Mater. Sci. 31 (1996) 1879.
[39] C.D. Wagner, Practical Surface Analysis in Auger and X-ray Photoelectron spectroscopy, vol. 1, Wiley, Chichester, 1994, p. 595.
[40] G. Beamson, D. Briggs, High-resolution XPS of Organic Polymers. The Scienta ESCA300 Database, Wiley, Chichester, 1992.
[41] G. Ertl, H. Knözinger, J. Weitkamp (Eds.), Handbook of heterogeneous catalysis, Wiley–VCH, Weinheim, 1997, p. 5.
[42] A.J. Wagner, G.M. Wolfe, D.H. Fairbrother, Appl. Surf. Sci. 219 (2003) 317 (and refs. therein).
[43] C. Baker, S. Ismat Shah, S.K. Hasanain, J. Magn. Magn. Mater. 280 (2004) 412.
[44] Yu.A. Barnakov, B.L. Scott, V. Golub, L. Kelly, V. Reddy, K.L. Stokes, J. Phys. Chem. Solids 65 (2004) 1005.
[45] A. Petri-Fink, M. Chastellain, L. Juillerat-Jeanneret, A. Ferrari, H. Hofmann, Biomaterials 26 (2005) 2685.